Influence of interplanetary solar wind sector polarity on the ionosphere

Jing Liu,[1,2] Libo Liu,[1] Biqiang Zhao,[1] and Weixing Wan[1]

Received 21 April 2012; revised 21 June 2012; accepted 17 July 2012; published 30 August 2012.

[1] Knowledge of solar sector polarity effects on the ionosphere may provide some clues in understanding of the ionospheric day-to-day variability and "hysteresis" effect on foF2. Ionospheric response to changes in solar sector polarity has not been fully documented previously, partly due to the limitation of observations. In this study, a solar-terrestrial connection ranging from solar sector boundary (SB) crossings, geomagnetic disturbances and ionospheric perturbations has been demonstrated. The increases in interplanetary solar wind speed within three days are seen after SB crossings, while the decreases in solar wind dynamic pressure and magnetic field intensity immediately after SB crossings are confirmed by the superposed epoch analysis results. Furthermore, the interplanetary magnetic field (IMF) Bz component turns from northward to southward in March equinox and June solstice as the Earth passes from a solar sector of outward to inward directed magnetic fields, whereas the reverse situation occurs for the transition from toward to away sectors. The IMF Bz component for the same solar sector polarity has opposite signs between March equinox and September equinox, and also between June solstice and December solstice. In order to know how the ionosphere reacts to the interplanetary solar wind variations linkage of SB crossings, the F2 region critical frequency (foF2) covering about four solar cycles and total electron content (TEC) during 1998–2011 are utilized to extract the related information, revealing that they are not modified significantly and vary within the range of $\pm$15% on average. The responses of the ionospheric TEC to SB crossings exhibit complex temporal and spatial variations and have strong dependencies on season, latitude, and solar cycle. This effect is more appreciable in equinoctial months than in solstitial months, which is mainly caused by larger southward *Bz* components in equinox. In September equinox, latitudinal profile of relative variations of foF2 at noon is featured by depressions at high latitudes and enhancements in low-equatorial latitudes during IMF away sectors. The negative phase of foF2 is delayed at solar minimum relative to it during other parts of solar cycle, which might be associated with the difference in longevity of major interplanetary solar wind drivers perturbing the Earth's environment in different phases of solar cycle.

Citation: Liu, J., L. Liu, B. Zhao, and W. Wan (2012), Influence of interplanetary solar wind sector polarity on the ionosphere, *J. Geophys. Res.*, *117*, A08335, doi:10.1029/2012JA017859.

1. Introduction

[2] The solar sector boundary (SB), which is intersected by the ecliptic plane with the heliospheric current sheet, separates the sectors in which the orientation of radial (Bx) and azimuthal (By) components of interplanetary magnetic field (IMF) changes from away (toward) to toward (away) the sun. It was demonstrated in previous works [*Mendoza and Enríquez*, 1995; *Echer and Gonzalez*, 2004] that there is an intimate relationship between SB crossings and geomagnetic activities. IMF Bz component serves as a crucial factor to understand the IMF sector related solar-terrestrial phenomena since the solar wind energy transfer into the magnetosphere is favored by the negative IMF Bz component and resisted by the positive Bz component. A northward or southward Bz component could be generated due to the inclination of the current sheet with respect to the ecliptic surface. As revealed by *Bremer* [1988], the orientation of Bz component in the Geocentric Solar Magnetospheric (GSM) coordinate in the IMF sector polarity have a strong dependence on season. For example, IMF sectors with outward directed magnetic fields will produce northward Bz components in March equinox and southward Bz components in September equinox in the GSM coordinate. This effect is

[1]Beijing National Observatory of Space Environment, Institute of Geology and Geophysics, Chinese Academy of Sciences, Beijing, China.
[2]Graduate University of Chinese Academy of Sciences, Beijing, China.

Corresponding author: L. Liu, Institute of Geology and Geophysics, Chinese Academy of Sciences, Beijing 100029, China (liul@mail.iggcas.ac.cn)

0148-0227/12/2012JA017859

Table 1. List of the Ionosonde Stations From Which Ionospheric Data Are Used

Station	Code	Geographic Latitude (deg)	Geographic Longitude (deg)	Magnetic Latitude (deg)
Yakutsk	YA462	62.0	129.5	51.3
Irkutsk	IR352	52.5	104.0	41.2
Wakkanai	WK545	45.4	141.7	35.5
Akita	AK539	39.7	140.1	29.9
Kokubunji	TO535	35.7	139.5	25.9
Wuhan	WU430	19.5	114.4	19.5
Manila	MN414	14.6	121.1	3.8
Slough	SL051	51.5	359.4	54.0

most pronounced in equinox [*Russell and MacPherron*, 1973]. Additionally, it has been established that the transient of SB at Earth is usually followed by high-speed streams and resultant geomagnetic activity enhancement [*Smith*, 2001; *Crooker et al.*, 2004; *Khabarova and Zastenker*, 2011].

[3] The Earth's upper atmosphere can be disturbed by the solar wind energy dissipation in accompany of SB crossing the Earth due to its geoeffectiveness [*Echer and Gonzalez*, 2004]. Enhanced auroral Joule heating and particle precipitations will change the neutral composition and drive the thermosphere in motion. The upwelling neutral atmosphere brings molecule-rich air from lower thermosphere to higher altitudes decreasing O/N2 ratio in the upper thermosphere, which have important implications to ionospheric electron density in the *F* region. Because an increase in the N2 density increases the loss rate of ionization and a decrease in the O density reduces its production. The regions with decreased O/N2 expand toward the equator in the postmidnight sector and then corotate with Earth into the dayside [*Prölss*, 1995]. Moreover, pressure-gradient force set up by auroral energy injection changes the global thermospheric circulation. Modification in the thermospheric circulation will generate disturbance dynamo electric field through disturbance dynamo process [*Blanc and Richmond*, 1980]. Observations showed that noon time equatorial electric field was altered by the disturbance dynamo electric field in connection with the IMF polarity alternations [e.g., *Sastri*, 1989].

[4] Not many studies have been carried out previously on the ionospheric and thermospheric responses to SB crossings. It was first found by *Low et al.* [1975] that the appearance of ~6 and ~15 days periods in ionospheric electron density had an association with interplanetary SB crossing. *Wilcox* [1979] reported that transients of sector boundary may change the tropospheric circulation. Later, *Mendillo and Schatten* [1983] employed a latitudinal chain of total electron content (TEC) observations around 70°W meridian to assess the impacts of SB crossings. Their results suggested that the influence of these crossings on the ionosphere is merely attributed to small-scale geomagnetic storm effects. Studies of the impacts of SB crossings on ionospheric F2 layer critical frequency (foF2) have demonstrated that these effects show seasonal, local time, and solar activity dependencies [e.g., *Bremer*, 1988]. *Laštovička* [1986] analyzed the influence of the interplanetary SB crossings on the winter ionosphere and found that the whole ionosphere was affected except for the daytime lower ionosphere. Records relevant to solar sector polarity are not only registered in the ionosphere, but also in the thermosphere. Most recently, *Kwak et al.* [2011] performed an analysis of the thermospheric density response to the variations in IMF sector polarity, demonstrating that high-latitude thermospheric mass density at 400 km increases (decreases) in the toward (away) sector in the September equinox. As a response to the same solar polarity, thermospheric variations present almost the opposite behaviors in March equinox compared to them in September equinox.

[5] In spite of these efforts, global signatures of ionospheric TEC and foF2 responses to SB crossings remain incompletely documented. As advocated by *Mendillo and Schatten* [1983] and *Mendillo* [2006], it is worthwhile to survey these repeatable features which are well-organized by SB crossings, shedding lights on the prediction of ionospheric relevant perturbations. The aim of this work is to perform a systemic analysis of the influences of the changes in IMF polarities on the ionospheric foF2 and TEC in terms of their seasonal, solar cycle, local time and latitudinal dependencies. It has the merits in explaining the unresolved problem-"hysteresis" effect on foF2; that is, foF2 may have different values at the same solar activity level during different phases of a solar cycle [*Liu et al.*, 2011].

2. Data and Methods

[6] The ionospheric F2 region critical frequency (foF2) is routinely scaled at the ionosonde stations in the East Asia. The station information is given in Table 1. Data at Wuhan are obtained from Wuhan Ionospheric Observatory of the Institute of Geology and Geophysics of the Chinese Academy of Sciences, and data at Irkutsk and Yakutsk are from the Institute of Solar-Terrestrial Physics of Russia. Observations of foF2 from several ionosonde stations in Japan are provided by the National Institute of Information and Communications Technology (http://wdc.nict.go.jp/cgi-bin/print/manual_src/m_wrk/m_wrk). Other ionosonde foF2 data are collected from the SPIDR website (http://spider.ngdc.noaa.gov/).

[7] Global Ionospheric Maps (GIMs) of the JPL-provided Ionospheric Maps Exchange Files (IONEX) during the years 1998–2011 are used in the current analysis [e.g., *Iijima et al.*, 1999; *Mannucci et al.*, 1998]. The Kalman filter algorithm is adopted to solve the values of hardware biases and the ionospheric vertical TEC (VTEC) maps. The GIMs TEC provided by JPL has a two-hour temporal resolution and a spatial resolution of 5° in longitude and 2.5° in latitude. Before the day 307, 2002, each daily IONEX file contains 12 VTEC maps, beginning from 01:00 UT to 23:00 UT. The new files after the day 307, 2002 include 13 VTEC maps in every day, starting from 00:00 UT to 24:00 UT. We follow the methods of *Codrescu et al.* [2001] to construct TEC maps in the coordinate of magnetic local time (MLT) and magnetic latitudes (MLAT). Thus, we transform the geographic longitude and latitude into MLT and MLAT, and divide the MLT versus MLAT coordinate into mesh grids with a grid length dMLAT = 1 h and dMLAT = 2.5° as our previous works [e.g., *L. Liu et al.*, 2010]. TEC used in the present work is only from the Northern Hemisphere where GPS receivers have denser distributions.

[8] The same methods as *Mendillo and Schatten* [1983] have been adopted to highlight SB crossing effects on the

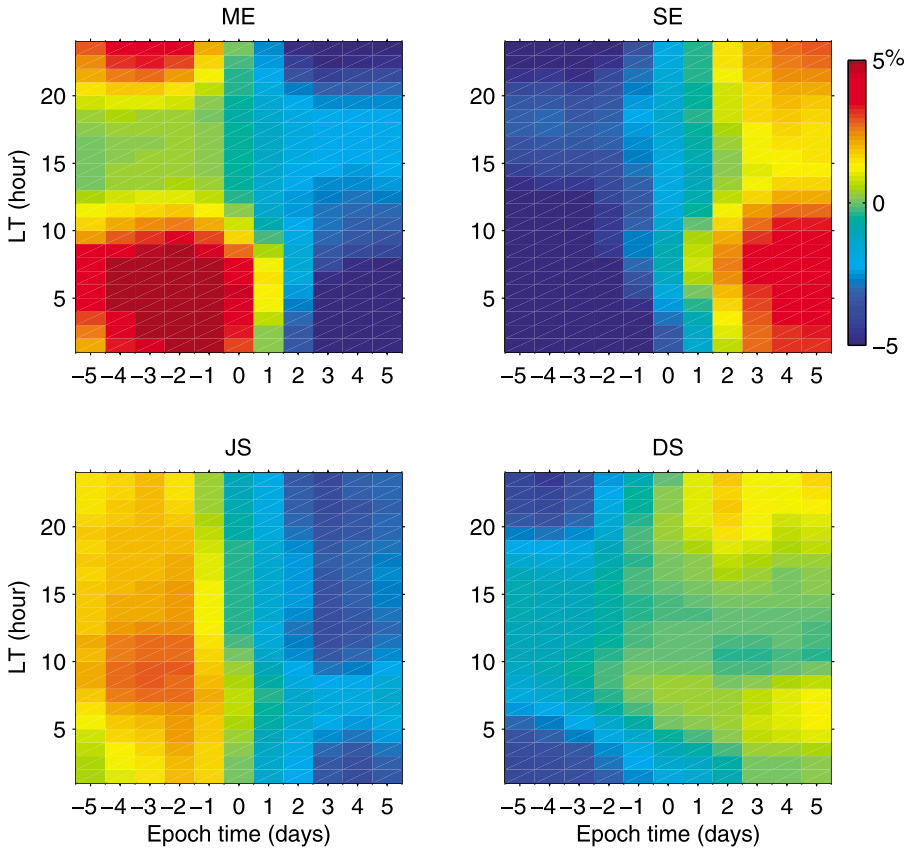

Figure 1. Supposed epoch analyses of RfoF2 (%) at different local times and seasons during IMF sector boundary crossing from away to toward sectors. The zero epoch time is set to the time of solar wind sector boundary crossings. The data is obtained from the ionosonde station Slough (51.5°N, 359.4°E). ME, SE, JS, and DS stand for March Equinox, September Equinox, June Solstice, and December Solstice, respectively.

ionospheric foF2 and TEC. Relative variations in percentage of foF2 (RfoF2 (%)) in each ionosonde station at any moment with respect to their 27-day moving median values are calculated. In the MLT versus MLAT coordinate, we use the same way to compute the relative deviations of TEC (RTEC (%)) in every grid point. The daily mean RTEC map can be retrieved by averaging the 12 or 13 RTEC maps of each day. Then daily averaged RTEC map as a function of MLAT and MLT are organized on universal time in a superposed epoch manner. The day of SB crossing is set to the zero epoch time. The RTEC maps before and after the zero epoch time are averaged separately; that is, 5-day RTEC maps locating in the same solar polarity are averaged. The mean patterns of RTEC (%) in the Northern Hemisphere during the IMF away sector (top) and toward sector (bottom) are depicted in Figure 6. Similarly, RfoF2 at a fixed local time are arranged covering 5 days before and after the zero epoch time. The superposed epoch analysis method has the advantage in enhancing signals and suppressing noises. The SB lists are obtained from Leif Svalgaard's list (http://www.leif.org/research/) and OMNI web list (http://omniweb.gsfc.nasa.gov/html/polarity/polarity_tab.html), containing 1335 events during the periods of available OMNI 2 data (ftp://nssdcftp.gsfc.nasa.gov/spacecraft_data/omni/) from January 1964 to December 2011. These lists were applied in the other works as well [*Echer and Gonzalez*, 2004; *Khabarova and Zastenker*, 2011].

3. Results

3.1. IMF Polarity Effects on foF2 and Its Seasonal and Local Time Dependencies

[9] Figure 1 shows the superposed epoch results of RfoF2 (%) at Slough (51.5°N, 359.4°E) in the frame of local time (LT) and seasons during the IMF SB crossings from away to toward sector condition. The IMF is separated by the ecliptic plane into two opposite magnetic sector polarities. "toward" sectors and "away" sectors denote the sectors where IMF Bx > 0 and Bx < 0, respectively, in the GSM coordinate where positive *x* axis points to the sun. ME, SE, JS, and DS are abbreviations of March Equinox, September Equinox, June Solstice, and December Solstice, respectively. There are apparent seasonal and local time dependencies of the ionospheric variations as the Earth travels from the away to toward solar sectors. The induced changes in foF2 are not very pronounced but with a clear transition from relatively enhanced to relatively depleted states in ME and JS; nevertheless, almost the reverse trends hold in SE and DS. The overall diurnal pattern of the SB crossing effects on the foF2 is a relative consistent one, but more obvious negative

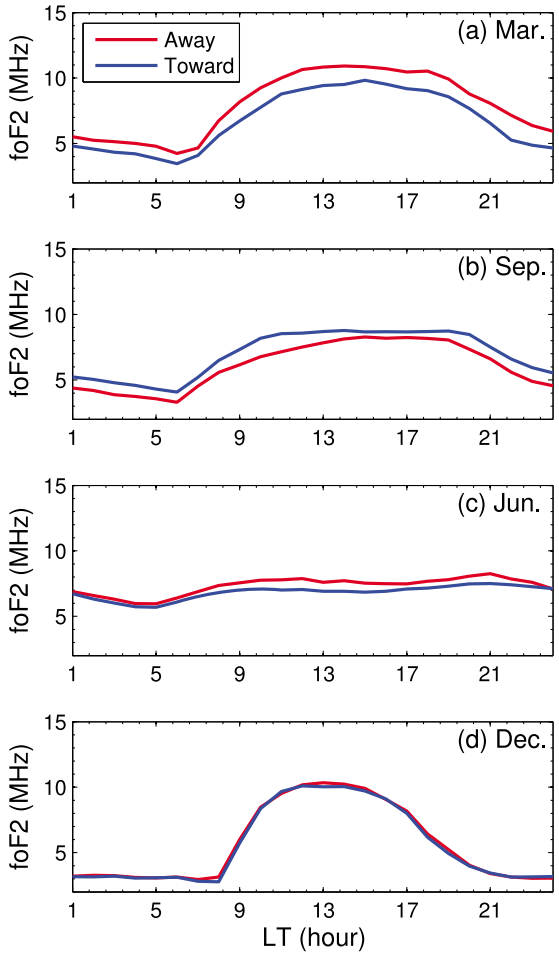

Figure 2. Average pattern of diurnal variations of foF2 at Slough during away (red line) and toward (blue line) polarities of the IMF.

phases of foF2 appear at the midnight to the early morning sector in ME when the Earth locates in the "toward" sectors.

[10] As regard to seasonal dependence of this effect, as depicted in Figure 1, SB crossing induced depletion is more remarkable in equinoctial months than that in solstitial months, which is consistent with the previous findings [e.g., *Mendillo and Schatten*, 1983; *Bremer*, 1988]. Moreover, the variations of foF2 differ in response to the SB crossing between ME and SE. There is a tendency of foF2 altering from a reduced state into an increased state in SE, which is almost opposite to the characteristics in ME. In ME, relative deviation of foF2 peaks around 2–3 days before the zero epoch time with an order of about 8% enhancement relative to its 27-day moving median value, minimizing at around 4th day after the zero epoch time. Percentage changes of foF2 in JS are reminiscent of them in ME but with weaker amplitudes, and exhibit contrasting behaviors in DS. Almost the reverse patterns occur during the SB crossing from toward to away sectors (not shown here) with respect to them during the SB crossing from away to toward sectors. To avoid repetition, we only adopt the cases of an "away" followed by a "towards" sector.

[11] In order to further demonstrate the seasonal dependence of the IMF SB crossing effects on foF2 over Slough, the mean diurnal variations of foF2 in each month at the moderate solar activity conditions (140 < =F10.7 < =160, in units of 10^{-22} W m^{-2} Hz^{-1}) during 1963–2011 have been presented in Figure 2. As depicted in Figure 2, in March and June, foF2 tends to be larger in the anti-sunward IMF polarity (red line) than that in the sunward (blue line) IMF polarity, which is in accordance well with the results derived by *Bremer* [1988]. Nevertheless, sector polarity influence is almost indiscernible in December, and it is stronger at high latitudes [e.g., *Bremer*, 1988]. Using foF2 in during 1966–1973, *Laštovička and Křivský* [1985] found that the effect of the discrepancy between IMF away and toward sectors is negligible in winter midlatitudes. This indicates that the observed foF2 at different latitudes are subject to distinct modifications by SB crossings.

3.2. Solar Cycle and Latitudinal Dependencies of the Ionospheric Response to SB Crossings

[12] Figure 3 plots the curves of yearly moving mean of F10.7 index in units of 10^{-22} W m^{-2} Hz^{-1} and foF2 (MHz) at 1200 LT during 1948–2008. The solar activity varies with about 11-year periodicity and foF2 follows this tendency closely. In the upper panel, four kinds of line color are used to identify the different phases of the solar cycle: rising (green), falling (blue), maximum (red), minimum (black).

[13] In order to check if the ionosphere responds distinctly to SB crossings in different portions of the solar cycle, Figure 4 illustrates the superposed epoch results of RfoF2 (%) at Slough within different phases of solar cycle during IMF solar sector crossing from inward/outward to outward / inward conditions. Only the cases at noon in ME when this impact is most pronounced are taken into account. Similarity and difference exist in different parts of solar cycle in response to SB crossings. The ionospheric foF2 undergoes a change from relatively enhanced to relatively depleted state as the Earth passes from the away to toward sectors regardless of the phase of solar cycle, while the reverse pattern occurs when the solar polarities change from toward to outward directions. The time of achieving minimum is different. At solar maximum, relative difference of foF2 decreases to the lowest level ~6% in the first day after SB crossing, saturates in the following days, and minimizes at the second day at solar rising and falling phases. At solar minimum, the moment with the greatest reduction of relative difference of foF2 being an order of 6% is postponed to the 4th day after the zero epoch time.

[14] In the process of IMF sector polarity transiting from toward to away sectors, the ionospheric RfoF2 tends to start from negative values to positive ones. The relative deviations of foF2 relative to their 27-day running mean are within ±8%. The greatest increment appears in the solar rising phase, which coincides with situations during the IMF sector polarity changing from the away to toward sectors. Based on the ionosonde observations at two geophysically equivalent sites located at subauroral latitudes during 1964–1976, *Mendillo and Narvaez* [2009] studied the ionospheric storms in different phases of the solar cycle, revealing that the storm-time ionosphere experienced the deepest depression at solar maximum. As we know, strong geomagnetic storms occur more often at solar maximum. In general, stronger geomagnetic storms tend to disturb the ionosphere to a greater extent owing to larger auroral energy dissipations. Therefore the

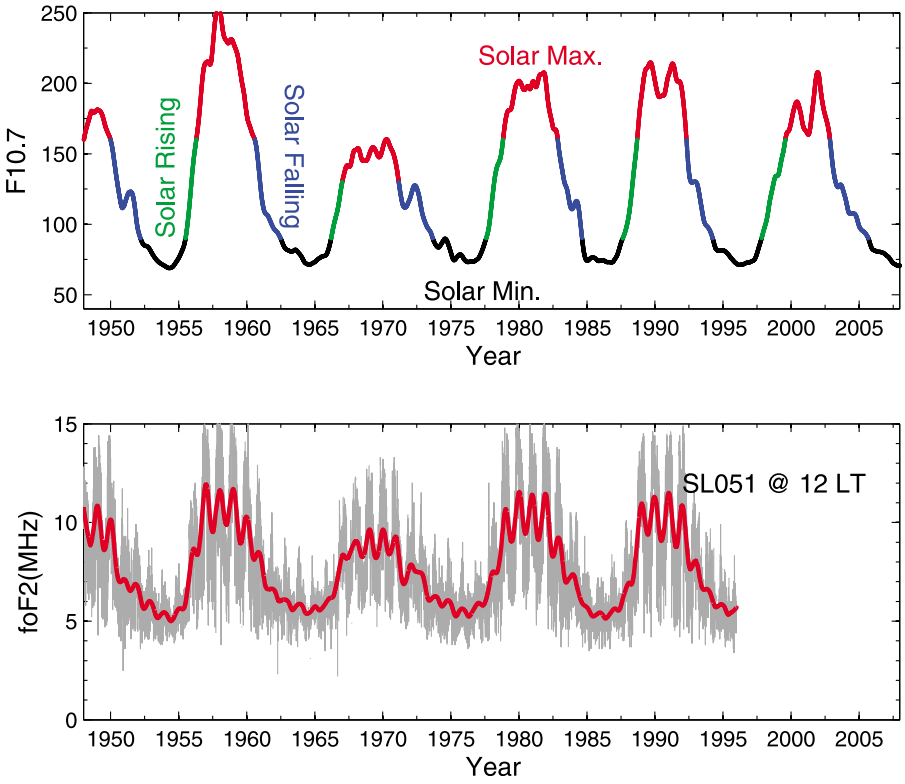

Figure 3. Yearly moving mean of F10.7 index in units of 10^{-22} W m^{-2} Hz^{-1} and foF2 at 1200 LT. In the top panel, the different colors are used to identify the different phases of the solar cycle.

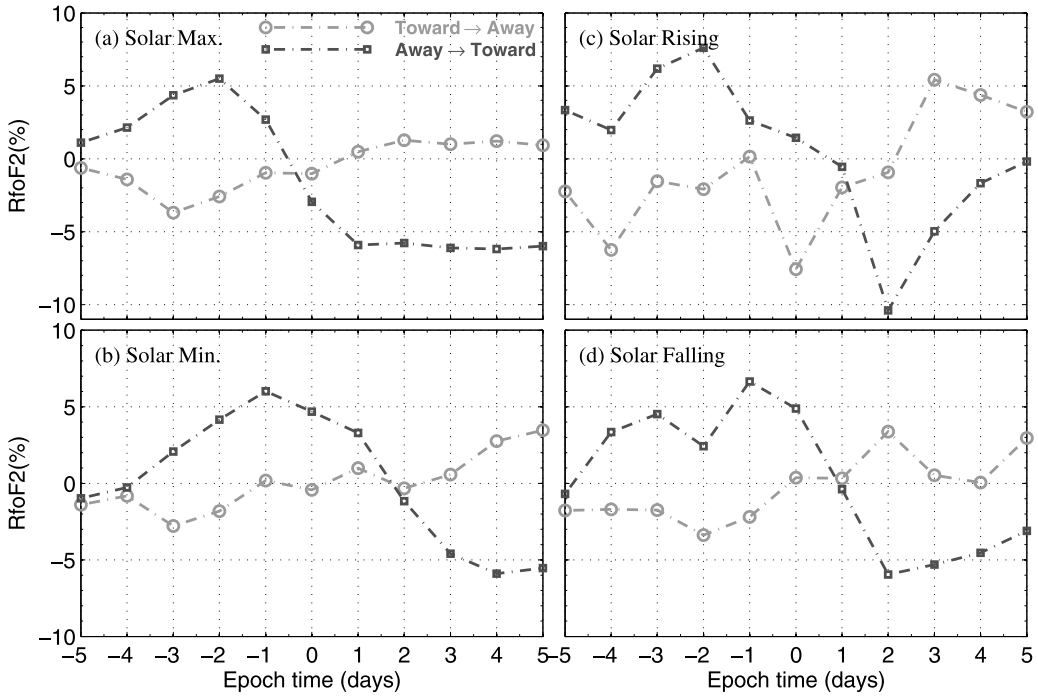

Figure 4. Superposed epoch analyses of RfoF2 (%) at Slough in ME at different portions of solar cycle during IMF sector boundary crossing from toward to away sectors (gray) and from away to toward sectors (black).

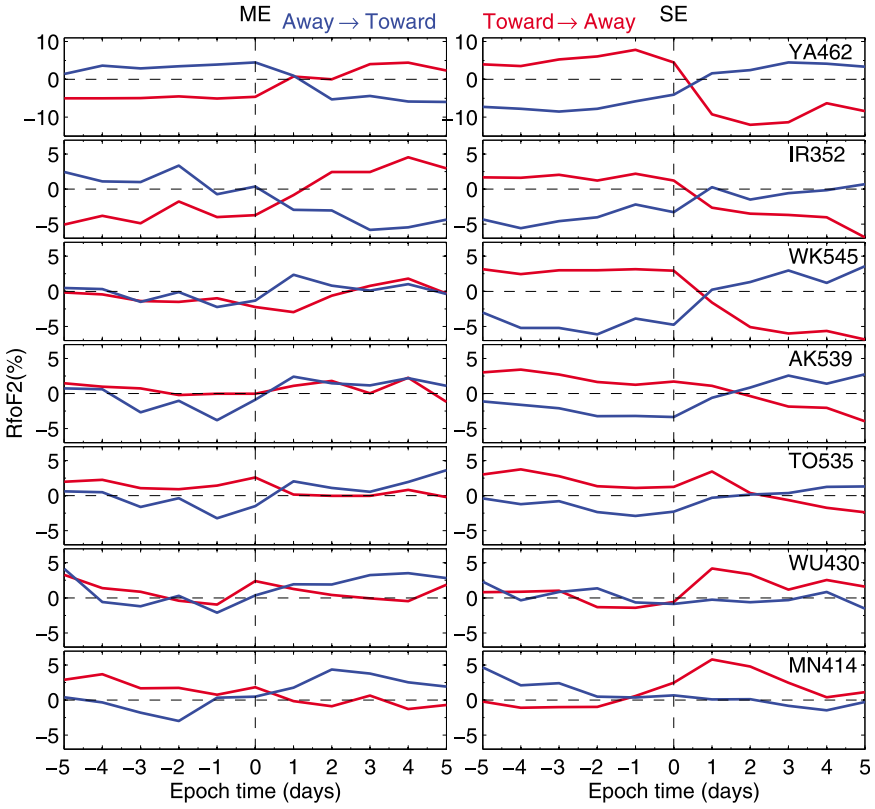

Figure 5. Latitudinal variations of the superposed epoch results of noontime RfoF2 (%) in SE and ME during IMF sector boundary crossing from toward to away (red line) sectors and away to toward (blue line) sectors.

storm-time ionospheric electron density should depart from the quiet time state most at solar maximum with respect to them during other phases of the solar cycle. Nevertheless, SB crossings impacts on the ionospheric foF2 are most remarkable at the rising phase, being distinction from results of *Mendillo and Narvaez* [2009]. The primary reasons for this discrepancy are still not clear.

[15] To examine the latitudinal variation of the IMF SB crossing effects on ionospheric foF2, data provided by ionosonde stations situated between the auroral region and the dip equator in the East Asia are analyzed. The observed noontime foF2 in ME and SE during the years 1964–1988 when these ionosonde stations have good data coverage are used in this section. In SE, it is shown in Figure 5 that RfoF2 are greater at high-middle latitudes during toward sectors than it during outward sectors. In the same season, IMF polarity effects are more remarkable at high and low latitudes and delayed at lower latitudes. For instance, the largest decrease after the zero epoch time over YA462 approximates 10% on the 3rd day, and it attains the minimum ~5% on the 4th day over WK545. A changeover of this tendency takes place at low-equatorial latitudes, commencing at the Wuhan ionosonde station. Ionospheric *F* region critical frequency after the zero epoch time switches from the relatively depleted state to the relatively enhanced states.

[16] In ME, ionospheric foF2 at high and low-equatorial latitudes display almost the opposite trend with respect to them in SE. At high latitudes, ionospheric foF2 in ME are decreased in toward sectors. At middle latitudes, the ionospheric variations of foF2 in ME are not apparent (i.e., foF2 at WK545 and AK539 seems almost unchanged during the transition from the toward to away sectors). In the equatorial ionosphere, the foF2 in ME is inclined to attain larger values in the IMF toward polarity.

3.3. The Influence of SB Crossings on TEC

[17] Figure 6 depicts the average percentage differences of TEC in the Northern Hemisphere during the IMF away sector (upper panel) and toward sector (lower panel) conditions. Here we mainly focus on the large-scale and pronounced variations of TEC. In the away sector, as shown in upper panels of Figure 6, the TEC reduces by about 10% at high latitudes in SE and DS and this region expands more equatorward in SE and DS than in JS, which seems to contradict with current understanding of ionospheric storm effects since one would expect that negative ionospheric storm effects caused by thermospheric composition disturbance bulge is easier brought to lower latitudes in summer by the summer-to-winter prevailing winds [*Fuller-Rowell et al.*, 1996]. A narrow arc-shaped structure with increased TEC appears in nighttime ME at the auroral latitudes. In SE, the latitudinal profiles of TEC variations resemble the behavior of foF2 in Figure 5, featured by high latitude depression and low latitudes increment. It should be noted that the regions with enhanced or depleted TEC should be considered as relative changes that happening due to the removal of a 27 day moving median value.

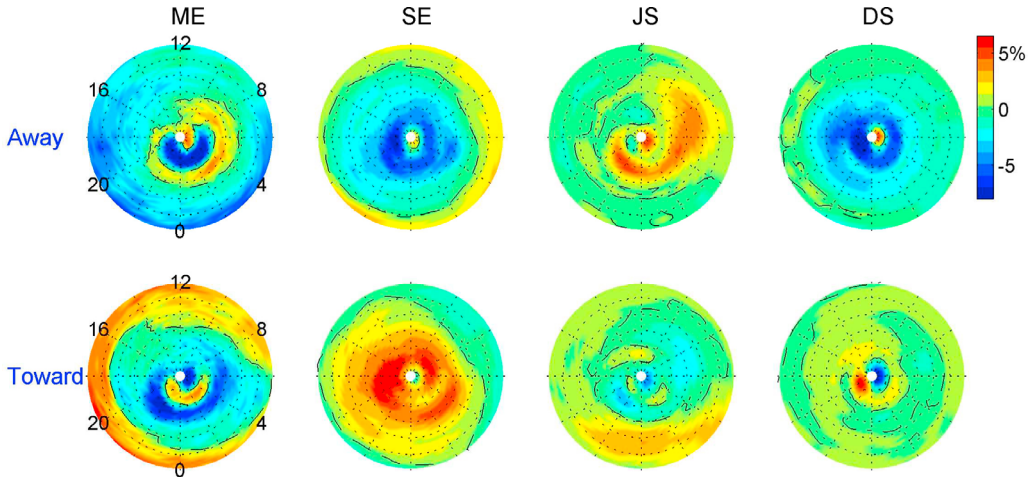

Figure 6. Average patterns of RTEC (%) in the Northern Hemisphere during the IMF (top) away sector and (bottom) toward sector conditions.

[18] Now we focus our attention on the toward sectors' effects on the ionosphere. An apparent negative phase of TEC at high-middle latitudes mainly takes place in ME and JS. In SE, the TEC increases by ~8% at high latitudes, while this effect is not so obvious in DS. In JS and ME, the negative phase expands most equatorward to around 30° magnetic latitude in the early morning sector when it is conducive to equatorward propagation of the negative phase in TEC. This signature is in conformity with that observed in ionospheric storm effects [e.g., *Zhao et al.*, 2007; *Liu et al.*, 2010a]. These characteristics mentioned above will be interpreted in the discussion part.

4. Discussion

[19] As revealed by *Forbes et al.* [2000] and *Rishbeth and Mendillo* [2001], on average, daily variations of F2-layer electron density have a standard deviation of 20% by day and 33% by night at medium solar activity. *Mendillo et al.*, [1983] has proven that the derived average patterns in association with SB crossing impacts on the ionosphere are reliable and stable through assessing the significance of results in the following methods. On the one hand, their statistical results indicated that the peak amplitudes of ionospheric variations during SB crossings are larger than the errors. On the other hand, the features seen in the ionosphere related to these crossings disappear if without discriminating the IMF polarity. Our results are consistent with the finding of *Mendillo et al.* [1983] in magnitude and the manners in response to SB crossing in some aspects. Moreover, the repeatability of ionospheric modifications and overall consistency between the ionospheric variations and interplanetary solar wind parameters give further evidences that the observed ionospheric patterns are due to the physical processes linked to solar polarity variations.

[20] The induced variations of ionospheric foF2 and TEC by SB crossing reflect the ionospheric response to the increased or decreased geomagnetic forcing. It is instructive to investigate the interplanetary solar wind conditions and resultant geomagnetic activity in each season, which is critical to understand the observed phenomena. As depicted in Figure 7, the average patterns of interplanetary solar wind velocity, dynamic pressure *P*, magnetic field intensity *B*, z component of magnetic field *Bz*, and geomagnetic index *Ap* during 1963–2010 are colored in red (blue) during IMF SB crossing from toward (away) to away (toward) sector conditions. While the increases in interplanetary solar wind speed within three days are observed after the zero epoch time, the decreases in dynamic pressure and magnetic field intensity are seen immediately after SB crossing in Figure 7. Variations of these parameters (V, P, B) are similar to the signatures observed during the passage of Corotating Interaction Regions (*CIRs*), which are formed by the interaction between high-speed solar winds and the background low-speed solar winds [*Tsurutani et al.*, 2006]. But the notable difference in the solar wind parameters between SB crossing and CIRs lies in that IMF Bz typical oscillates rapidly between northward and southward directions during the passage of CIRs [e.g., *Tsurutani et al.*, 2006; *Liu et al.*, 2012]. The observed IMF Bz in Figure 7 are quite stable in each solar sector. Furthermore, the variations of these parameters match the characteristics seen during the transitions of SB [e.g., *Khabarova and Zastenker*, 2011]. These make us believe that the ionospheric variations are mainly caused by SB crossings but not due to CIRs effects.

[21] The patterns of interplanetary *Bz* component and the geomagnetic index *Ap* are direct manifestations of the geoeffectiveness in conjunction with SB crossings. Due to the difference between the geocentric solar-eclipse (GSE) and GSM coordinates, IMF By component in the GSE coordinate has a positive or negative IMF Bz offsets in the GSM coordinate [*Russell and McPherron*, 1973]. The Bz component turns from northward to southward in ME and JS during the transition from the away to toward sector, whereas the opposite situation is true for the transition from the toward to away sectors. *Bremer* [1988] introduced the concepts "anti-" and "pro" sectors corresponding to the sectors with positive and negative Bz conditions, respectively. In the "pro" sectors, the Bz component is around −1.1 nT in equinox and about −0.5 nT in solstice. The

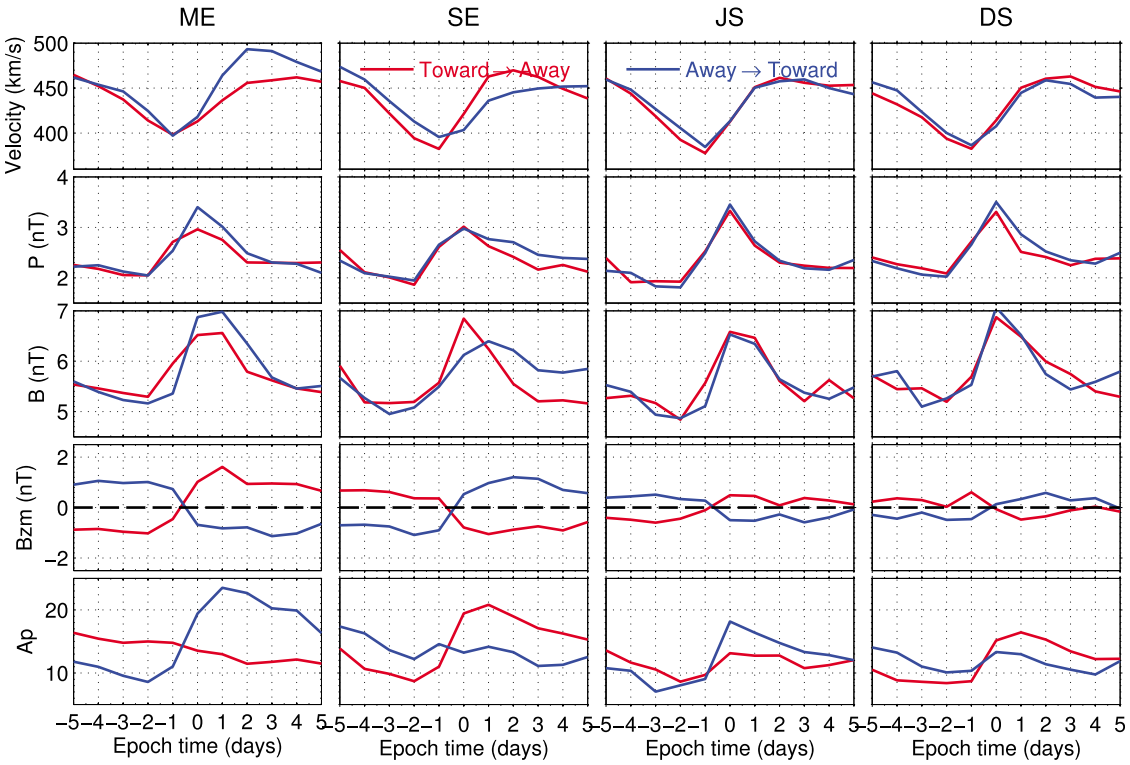

Figure 7. Mean variations of interplanetary solar wind velocity, dynamic pressure, magnetic field intensity, z component of magnetic field, and geomagnetic index Ap in 1963–2010 during IMF sector boundary crossing from toward to away sectors (red) and from away to toward sectors (blue).

seasonal variations of IMF SB crossing impacts on the ionospheric foF2 and TEC are closely linked to the energy transfer from the magnetosphere, which are largely controlled by seasonal variations of *Bz* component. We are now in a good position to interpret the influence of SB crossings on ionospheric variations.

[22] Since the first suggestion by *Seaton* [1956], it has been accepted that the decrease in electron density in the F region is typically attributed to the changes of neutral composition due to the heating of the thermosphere. Later, *Fuller-Rowell et al.* [1994, 1996] and *Prölss* [1995] extended this theory and accounted for the local time and seasonal variations of negative ionospheric storm effects. The neutral composition "bulge" generally forms in the nighttime sector, and is brought into low latitudes by storm-induced equatorward winds, and then corotates with the Earth into the dayside, and recovers partly in this process. This results in stronger reduction of electron density in the nighttime and early morning sectors relative to the daytime sector in the "pro" sectors as shown in Figures 1 and 6 in SE and ME.

[23] A salient feature concerning the seasonal dependence of the ionospheric modifications by SB crossings is that ionospheric foF2 at the sub-auroral latitude (Slough) experiences more pronounced perturbations in equinoctial months than in solstitial months. One would expect that the neutral composition disturbance bulge produces more remarkable effects in the summer high latitudes because of larger Joule heating rates in the Summer Hemisphere due to elevated electric conductivity [*Fuller-Rowell et al.*, 1996] and the prevailing summer-to-winter wind is favorable for neutral disturbance equatorward penetration in the Summer Hemisphere. This circumstance is largely determined by the southward IMF *Bz*, which serves as a key modulator in the solar wind energy transfer into the magnetosphere and corresponding ionospheric/thermospheric disturbances. According to the notion of *Russell and McPherron* [1973], geomagnetic activity generally peaks in equinox due to that IMF By component in GSE coordinate has a larger Bz component in the GSM coordinate in which the phenomena within the magnetosphere is well ordered. The enhanced geomagnetic activity may perturb the ionosphere to a greater extent as consequence of Joule heating and particle sedimentation. Thus it is not surprising to see in Figure 6 that a larger reduction in electron density in ME and SE than in JS because there is a larger southward *Bz* component in equinox. In addition, a marked difference of ionospheric modulation between the SE and ME arises from that IMF Bz offsets have different signs in the ME and SE, even though they belongs to the same solar sector polarity. As shown in Figure 7, in ME, there are positive and negative *Bz* components for the outward and toward sector polarity, respectively, whereas the reverse conditions apply to the condition in SE. This necessitates making a distinction between SE and ME in terms of dealing with SB crossings influences. The equinoctial asymmetry observed in the thermosphere and ionosphere [e.g., *Aruliah et al.*, 1996; *Balan et al.*, 1998; *L. Liu et al.*, 2010; *Kwak et al.*, 2011] is still unresolved issues. Unequal magnetospheric energy could be one of the plausible causes of equinoctial asymmetries in the

thermosphere and ionosphere, even though detailed physical sources of this asymmetry are unascertained.

[24] Generally, it is not an easy task for the neutral composition bulge to extend to the equator except for the largest superstorms [e.g., *Meier et al.*, 2005]. Thus the negative phase of ionospheric foF2 gradually turns into positive phase at noon in the equatorial-low latitudes as illustrated in Figures 5 and 6. At low-equatorial latitudes, several mechanisms can perturb this region involving disturbance electric fields, disturbance wind fields, waves, neutral composition changes. Disturbance electric fields can be divided into two categories: penetration electric field due to the leakage of magnetospheric electric fields and disturbance dynamo electric fields arising from interaction between disturbance winds and ionized species. The short-lived penetration electric field typically sustains no more than an hour [*Fejer*, 1991]. This makes this mechanism not operative for explaining the relative long-term variations in the ionosphere. Observations have proven the existence of disturbance dynamo electric fields [*Sastri*, 1989] as a result of IMF polarity related modulation, which is generally westward at the daytime and eastward at night. Under the influence of magnetic field, westward disturbance dynamo electric field at the daytime will generate the downward drifts of electron and inhibit the formation of daytime equator ionization anomaly and thus negative and positive phases at the crests and trough regions of the equatorial ionospheric anomaly, respectively. This process might only be responsible for the changes in the equator as illustrated in Figures 5 and 6. Therefore, other mechanisms should be involved in explaining the results. The most likely candidate is the increase O/N2 as a consequence of downwelling of neutral atmosphere because of the convergence of storm-induced circulation and background winds at low-equatorial latitudes [*Rishbeth et al.*, 1987; *Burns et al.*, 1995], resulting in an increase of *F* region electron density. In addition, disturbed equatorward neutral winds can be capable of enhancing the electron density at mid- and low latitudes [*Lin et al.*, 2005]. A changeover of this trend takes place at around 20° magnetic latitude [*Burge et al.*, 1973]. The equatorward wind alone will hinder the formation of the equatorial anomaly and thus produce the negative ionospheric storm effects at the crests region and positive storm effects at the equator.

[25] An intriguing phenomenon is displayed in Figure 4 in that the negative phase is delayed at solar minimum relative to it at solar maximum. We postulated that this is mainly caused by different dominant interplanetary solar wind drivers at different phases of the solar cycle. *Richardson et al.* [2002] examined the contributions of main solar wind structures (e.g., CIRs, slow solar wind, interplanetary coronal mass ejections (ICMEs), and shocks) to geomagnetic activity during 1972–2000, uncovering that CIRs becomes the primary interplanetary solar wind driver at solar minimum. For solar maximum periods, the transient structures such as ICMEs and shocks play a major role in the solar-terrestrial disturbance. CIRs-generated moderate geomagnetic activity generally persists for several days or even for up to the entire solar rotation [*Tsurutani et al.*, 1995; *Denton et al.*, 2006; *Liu et al.*, 2010b]. The durations of geomagnetic disturbance linked to ICMEs are unusually shorter in longevity than that of CIRs. Therefore, there is no wonder that the negative phase effects are postponed as well at solar minimum.

5. Conclusion

[26] In the current work, we have investigated the seasonal, solar activity, and latitudinal dependencies of SB crossings effects on the ionosphere. JPL-provided TEC and foF2 measured by ionosonde stations at around 130° meridian from auroral regions to equator are used to derive the solar polarity signals from them, which have intimate associations with the variations of Bz component. The results indicate that the SB polarity effects are not significant well within the range of ionospheric day-to-day variability [*Forbes et al.*, 2000; *Rishbeth and Mendilllo*, 2001] and have apparent seasonal, latitudinal, and solar activity dependencies. These effects are more noticeable in equinoctial months. Daytime latitudinal profile of relative variations of foF2 is characterized by high latitudes depression and low-equatorial latitudes enhancement. In the "pro" sector, the negative phase of foF2 is delayed at solar minimum with respect to it at other portions of solar cycle. The phenomena of TEC response to IMF SB polarity with negative Bz components are generally consistent with our current understanding of ionospheric storm effects.

[27] A solar-terrestrial chain from the solar sector boundary, geomagnetic disturbance, and ionospheric perturbations have been elucidated. This makes predications of the SB crossings induced ionospheric disturbances possible due to the well-organized sequences. In addition, the solar SB crossings do not induce significant changes in ionospheric parameters as geomagnetic storms or solar activity variations; however, it may be helpful for us to understand the day-to-day variability of the ionosphere [*Mendillo*, 2006].

[28] **Acknowledgments.** We acknowledge the access to the ionospheric observations and solar sector boundary lists. Ionospheric data are obtained from WDC for Ionosphere, Tokyo, National Institute of Information and Communications Technology, and from SPIDR. The JPL GIMs are downloaded from the Web site ftp://cddis.gsfc.nasa.gov. This research was supported by the Chinese Academy of Sciences (KZZD-EW-01-3), the National Key Basic Research Program of China (2012CB825604), National Natural Science Foundation of China (41074112, 41174137, 41174138), CMA grant GYHY201106011.

[29] Robert Lysak thanks the reviewers for their assistance in evaluating this paper.

References

Aruliah, A. L., A. D. Farmer, T. J. Fuller-Rowell, M. N. Wild, M. Hapgood, and D. Rees (1996), An equinoctial asymmetry in the high-latitude thermosphere and ionosphere, *J. Geophys. Res.*, *101*(A7), 15,713–15,722, doi:10.1029/95JA01102.

Balan, N., Y. Otsuka, G. J. Bailey, and S. Fukao (1998), Equinoctial asymmetries in the ionosphere and thermosphere observed by the MU radar, *J. Geophys. Res.*, *103*, 9481–9495, doi:10.1029/97JA03137.

Blanc, M., and A. Richmond (1980), The ionospheric disturbance dynamo, *J. Geophys. Res.*, *85*(A4), 1669–1686, doi:10.1029/JA085iA04p01669.

Bremer, J. (1988), The influence of the IMF structure on the ionospheric *F* region, *J. Atmos. Terr Phys.*, *50*(9), 831–838.

Burge, J. D., D. J. Eccles, W. King, and R. Rüster (1973), The effects of thermospheric winds on the ionosphere at low and middle latitudes during magnetic disturbances, *J. Atmos. Terr. Phys.*, *35*, 617–623, doi:10.1016/0021-9169(73)90192-X.

Burns, A. G., T. L. Killeen, W. Deng, G. R. Carignan, and R. G. Roble (1995), Geomagnetic storm effects in the low- to middle-latitude upper thermosphere, *J. Geophys. Res.*, *100*, 14,673–14,691, doi:10.1029/94JA03232.

Codrescu, M. V., K. L. Beierle, T. J. Fuller-Rowell, S. E. Palo, and X. Zhang (2001), More total electron content climatology from

TOPEX/Poseidon measurements, *Radio Sci.*, *36*, 325–333, doi:10.1029/1999RS002407.

Crooker, N. U., C.-L. Huang, S. M. Lamassa, D. E. Larson, S. W. Kahler, and H. E. Spence (2004), Heliospheric plasma sheets, *J. Geophys. Res.*, *109*, A03107, doi:10.1029/2003JA010170.

Denton, M. H., J. E. Borovsky, R. M. Skoug, M. F. Thomsen, B. Lavraud, M. G. Henderson, R. L. McPherron, J. C. Zhang, and M. W. Liemohn (2006), Geomagnetic storms driven by ICME- and CIR-dominated solar wind, *J. Geophys. Res.*, *111*, A07S07, doi:10.1029/2005JA011436.

Echer, E., and W. D. Gonzalez (2004), Geoeffectiveness of interplanetary shocks, magnetic clouds, sector boundary crossings and their combined occurrence, *Geophys. Res. Lett.*, *31*, L09808, doi:10.1029/2003GL019199.

Fejer, B. G. (1991), Low-latitude electrodynamic plasma drifts: A review, *J. Atmos. Terr. Phys.*, *53*, 677–693, doi:10.1016/0021-9169(91)90121-M.

Forbes, J. M., S. E. Palo, and X. Zhang (2000), Variability of the ionosphere, *J. Atmos. Sol. Terr. Phys.*, *62*, 685–693, doi:10.1016/S1364-6826(00)00029-8.

Fuller-Rowell, T. J., M. V. Codrescu, R. J. Moffett, and S. Quegan (1994), Response of the thermosphere and ionosphere to the geomagnetic storms, *J. Geophys. Res.*, *99*, 3893–3914, doi:10.1029/93JA02015.

Fuller-Rowell, T. J., M. V. Codrescu, H. Rishbeth, R. J. Moffett, and S. Quegan (1996), On the seasonal response of the thermosphere and ionosphere to the geomagnetic storms, *J. Geophys. Res.*, *101*, 2343–2353, doi:10.1029/95JA01614.

Iijima, B. A., I. L. Harris, C. M. Ho, U. J. Lindqwister, A. J. Mannucci, X. Pi, M. J. Reyes, L. C. Sparks, and B. D. Wilson (1999), Automated daily process for global ionospheric total electron content maps and satellite ocean altimeter ionospheric calibration based on Global Positioning System data, *J. Atmos. Sol. Terr. Phys.*, *61*, 1205–1218, doi:10.1016/S1364-6826(99)00067-X.

Khabarova, O., and G. Zastenker (2011), Sharp changes of solar wind ion flux and density within and outside current sheets, *Sol. Phys.*, *270*, 311–329, doi:10.1007/s11207-011-9719-4.

Kwak, Y.-S., K.-H. Kim, Y. Deng, and J. M. Forbes (2011), Response of thermosphere density to changes in interplanetary magnetic field sector polarity, *J. Geophys. Res.*, *116*, A11316, doi:10.1029/2011JA016938.

Laštovička, J. (1986), Effects of the interplanetary magnetic field sector structure in the winter ionosphere, *Stud. Geophys. Geod.*, *30*, 297–303, doi:10.1007/BF01645469.

Laštovička, J., and L. Křívský (1985), Effects of the IMF pro- and anti-sectors in the winter midlatitude ionosphere, *Stud. Geophys. Geod.*, *29*, 101–104, doi:10.1007/BF01586419.

Lin, C. H., A. D. Richmond, R. A. Heelis, G. J. Bailey, G. Lu, J. Y. Liu, H. C. Yeh, and S.-Y. Su (2005), Theoretical study of the low- and mid-latitude ionospheric electron density enhancement during the October 2003 superstorm: Relative importance of the neutral wind and the electric field, *J. Geophys. Res.*, *110*, A12312, doi:10.1029/2005JA011304.

Liu, J., B. Zhao, and L. Liu (2010a), Time delay and duration of ionospheric total electron content responses to geomagnetic disturbances, *Ann. Geophys.*, *28*, 795–805, doi:10.5194/angeo-28-795-2010.

Liu, J., L. Liu, B. Zhao, W. Wan, and R. A. Heelis (2010b), Response of the topside ionosphere to recurrent geomagnetic activity, *J. Geophys. Res.*, *115*, A12327, doi:10.1029/2010JA015810.

Liu, J., L. Liu, B. Zhao, J. Lei, J. P. Thayer, and R. L. McPherron (2012), Superposed epoch analyses of thermospheric response to CIRs: Solar cycle and seasonal dependencies, *J. Geophys. Res.*, *117*, A00L10, doi:10.1029/2011JA017315.

Liu, L., M. He, X. Yue, B. Ning, and W. Wan (2010), Ionosphere around equinoxes during low solar activity, *J. Geophys. Res.*, *115*, A09307, doi:10.1029/2010JA015318.

Liu, L., W. Wan, Y. Chen, and H. Le (2011), Solar activity effects of the ionosphere: A brief review, *Chin. Sci. Bull.*, *56*(12), 1202–1211, doi:10.1007/s11434-010-4226-9.

Low, N. C., T. H. Roelofs, and P. C. Yuen (1975), Electron content power spectral estimates: Periods of 2 days to 1/2 year, *Planet. Space Sci.*, *23*, 133–141, doi:10.1016/0032-0633(75)90074-4.

Mannucci, A. J., B. D. Wilson, D. N. Yuan, C. M. Ho, U. J. Lindqwister, and T. F. Runge (1998), A global mapping technique for GPS derived ionospheric total electron content measurements, *Radio Sci.*, *33*, 565–582, doi:10.1029/97RS02707.

Meier, R. R., G. Crowley, D. J. Strickland, A. B. Christensen, L. J. Paxton, D. Morrison, and C. L. Hackert (2005), First look at the 20 November 2003 superstorm with TIMED/GUVI: Comparisons with a thermospheric global circulation model, *J. Geophys. Res.*, *110*, A09S41, doi:10.1029/2004JA010990.

Mendillo, M. (2006), Storms in the ionosphere: Patterns and processes for total electron content, *Rev. Geophys.*, *44*, RG4001, doi:10.1029/2005RG000193.

Mendillo, M., and C. Narvaez (2009), Ionospheric storms at geophysically equivalent sites—Part 1: Storm-time patterns for sub-auroral ionospheres, *Ann. Geophys.*, *27*, 1679–1694, doi:10.5194/angeo-27-1679-2009.

Mendillo, M., and K. Schatten (1983), Influence of solar sector boundaries on ionospheric variability, *J. Geophys. Res.*, *88*(A11), 9145–9153, doi:10.1029/JA088iA11p09145.

Mendoza, B., and R. P. Enríquez (1995), Geoeffectiveness of the heliospheric current sheet, *J. Geophys. Res.*, *100*(A5), 7877–7880, doi:10.1029/94JA02867.

Prölss, G. W. (1995), Ionospheric *F* region storms, in *Handbook of Atmospheric Electrodynamics*, vol. 2, edited by H. Volland, pp. 195–248, CRC Press, Boca Raton, Fla.

Richardson, I. G., H. V. Cane, and E. W. Cliver (2002), Sources of geomagnetic activity during nearly three solar cycles (1972–2000), *J. Geophys. Res.*, *107*(A8), 1187, doi:10.1029/2001JA000504.

Rishbeth, H., and M. Mendillo (2001), Patterns of F2-layer variability, *J. Atmos. Sol. Terr. Phys.*, *63*, 1661–1680, doi:10.1016/S1364-6826(01)00036-0.

Rishbeth, H., T. J. Fuller-Rowell, and D. Rees (1987), Diffusive equilibrium and vertical motion in the thermosphere during a severe magnetic storm: A computational study, *Planet. Space Sci.*, *35*, 1157–1165, doi:10.1016/0032-0633(87)90022-5.

Russell, C. T., and R. L. McPherron (1973), Semiannual variation of geomagnetic activity, *J. Geophys. Res.*, *78*(1), 92–108, doi:10.1029/JA078i001p00092.

Sastri, J. H. (1989), Response of equatorial electric field to polarity of interplanetary magnetic field, *Planet. Space Sci.*, *37*, 1403–1408, doi:10.1016/0032-0633(89)90110-4.

Seaton, M. J. (1956), A possible explanation of the drop in F-region critical densities accompanying major ionospheric storms, *J. Atmos. Terr. Phys.*, *8*, 122–124, doi:10.1016/0021-9169(56)90102-7.

Smith, E. J. (2001), The heliospheric current sheet, *J. Geophys. Res.*, *106*, 15,819–15,831, doi:10.1029/2000JA000120.

Tsurutani, B. T., W. D. Gonzalez, A. L. C. Gonzalez, F. Tang, J. K. Arballo, and M. Okada (1995), Interplanetary origin of geomagnetic activity in the declining phase of the solar cycle, *J. Geophys. Res.*, *100*(A11), 21,717–21,733, doi:10.1029/95JA01476.

Tsurutani, B. T., et al. (2006), Corotating solar wind streams and recurrent geomagnetic activity: A review, *J. Geophys. Res.*, *111*, A07S01, doi:10.1029/2005JA011273.

Wilcox, J. M. (1979), Influence of the solar magnetic field on tropospheric circulation, in *Solar-Terrestrial Influence on Weather and Climate*, edited by B. M. McCormac and T. A. Seliga, pp. 149–159 D. Reidel, Hingham, Mass., doi:10.1007/978-94-009-9428-7_15.

Zhao, B., W. Wan, L. Liu, and T. Mao (2007), Morphology in the total electron content under geomagnetic disturbed conditions: Results from global ionosphere maps, *Ann. Geophys.*, *25*, 1555–1568, doi:10.5194/angeo-25-1555-2007.